

Anomalous melting behavior under extreme conditions: hard matter turning “soft”

Gianpietro Malescio^{1†}, Franz Saija^{2‡}, and Santi Prestipino^{1*}

¹ *Università degli Studi di Messina, Dipartimento di Fisica,
Contrada Papardo, 98166 Messina, Italy*

² *CNR-Istituto per i Processi Chimico-Fisici,
Contrada Papardo, 98158 Messina, Italy*

Abstract

We show that a system of particles interacting through the exp-6 pair potential, commonly used to describe effective interatomic forces under high compression, exhibits anomalous melting features such as reentrant melting and a rich solid polymorphism, including a stable BC8 crystal. We relate this behavior to the crossover, with increasing pressure, between two different regimes of local order that are associated with the two repulsive length scales of the potential. Our results provide a unifying picture for the high-pressure melting anomalies observed in many elements and point out that, under extreme conditions, atomic systems may reveal surprising similarities with soft matter.

Many atomic substances show anomalous melting features at high pressures, where the term “anomalous” is commonly used to underline any difference with respect to standard, simple-fluid-like melting^{1,2,3}. However, some rare gases (usually assumed as prototypical simple fluids) already deviate from this idealized behavior: the slope dT/dP of Ar, Kr and Xe melting lines shows a substantial decrease for high pressures with respect to predictions based on corresponding-state scaling from the Ne melting curve⁴. For other materials, the melting line $T_m(P)$ shows an extended plateau (e.g. Ta, Mo, Cr⁵) or even a maximum, followed by a region of reentrant melting (e.g. Cs, Rb, Na, Te, H, N^{6,7,8,9,10,11,12,13}). In some cases (e.g. Cs, K, Ba, Na^{6,8,10,14}), a further pressure increase results in a positive melting slope again. As advances in experimental methods allow to reach higher and higher pressures, the class of substances exhibiting melting anomalies constantly expands and materials that not long ago were thought to undergo “normal” melting reveal instead an anomalous behavior (e.g. Na⁸).

Melting features that are similar to those outlined above are known to occur for classical pair interactions with a soft-repulsive component^{15,16,17,18,19,20,21,22,23}, used for modeling colloidal suspensions and to study liquid-liquid transitions and water-like anomalies. The crucial feature of such interactions is the existence of a range of interparticle distances where the strength of the repulsive force *reduces* as the distance gets smaller (core-softening condition²⁴). The relevance of soft interactions for the high-pressure behavior of real substances has received little attention so far since atoms are usually thought to be “hard” objects. Yet, as will be argued below, extremely high pressures may bring this common belief into question. In order to explore the nature of melting at such high pressures, we take a coarse-grained view of the problem and consider a classical potential that is widely used to calculate the equation of state of materials under extreme conditions, i.e., the Buckingham or exp-6 potential²⁵,

$$u(r) = \begin{cases} +\infty & , \quad r < \sigma_M \\ \frac{\epsilon}{\alpha-6} \left[6 e^{-\alpha(\frac{r}{\sigma}-1)} - \alpha \left(\frac{\sigma}{r} \right)^6 \right] & , \quad r \geq \sigma_M \end{cases} \quad (1)$$

where r is the interparticle distance, ϵ is the depth of the attractive well, σ is the position of the well minimum, α (usually taken in the range 10-15²⁶) controls the steepness of the short-range repulsion, and σ_M is the point where the function in the second line of (1) attains its maximum value ϵ_M . It has been noted that the exp-6 model accounts for high-pressure effects in much better way than other more popular models (e.g. the Lennard-Jones model)

owing to its less steep repulsion²⁷. However, the ability of the exp-6 interaction to satisfy the core-softening condition (see Fig. 1) has not been pointed out so far and its phase behavior was investigated only in a restricted range of pressures and temperatures where no melting anomaly occurs^{27,28,29}.

Using standard simulation methods (*NPT* Metropolis Monte Carlo in conjunction with Widom and Frenkel-Ladd free-energy methods³⁰), we computed the exp-6 phase diagram for a given α (choosing initially $\alpha = 11$) over a wide range of pressures P and temperatures T (expressed throughout the text in units of ϵ/σ^3 and ϵ/k_B , respectively). Our samples contained a number N of particles of the order of 1000 (finite-size corrections are negligible). As shown in Fig. 2, the melting line starts at low P with a positive slope that gradually reduces with increasing pressure until it vanishes at a point of maximum melting temperature T_M . This is followed by a pressure interval where dT_m/dP is negative. Eventually, at extremely high pressures, $T_m(P)$ recovers a positive slope. In order to discuss the phase diagram, assume for instance to increase P at fixed temperature (say $T = 8$). The system, initially fluid, becomes denser and denser with increasing pressure until it crystallizes into a face-centered cubic (FCC) solid. Upon increasing P further, the FCC solid undergoes a transition into a body-centered cubic (BCC) solid (FCC goes over into BCC also upon heating at constant pressure). This effect is related to a decrease in the mean nearest-neighbor distance with increasing pressure (or temperature), which brings particles to experience inner, less steep regions of the interaction potential (it is known that fluids interacting via an inverse-power law, $u(r) \propto r^{-n}$, do crystallize into a BCC solid for $n \lesssim 7$ while the solid phase is FCC for steeper repulsions³¹). When P is large enough, the BCC solid finally melts into a denser fluid. This follows from increasing competition, upon compression, between two separate scales of first-neighbor distance, i.e., a larger one associated with the soft repulsion (effective at the lower pressures) and a smaller one related to the particle-core diameter σ_M (dominant at the higher pressures). These two characteristic lengths push for different and incommensurate patterns of short-range order in the system, thus setting the stage for reentrance of the fluid phase at intermediate pressures (at least for not too low T). Upon further compression, the smaller length scale eventually takes over and the fluid crystallizes into a hard-sphere-like, FCC solid.

In the fluid region above the reentrant-melting line, isobaric cooling leads first to an increase in the number density ρ , followed by a decrease for further cooling (Fig. 2, inset).

The locus of points where ρ attains its maximum encloses a region of “density anomaly” (see Fig. 2). This has been observed under ordinary pressure in a number of systems, among which water is the most important³². Our findings raise the possibility that a density anomaly may as well occur at much higher pressures in those substances that are characterized by reentrant melting.

The above results are confirmed and further corroborated by an analysis of the system structure in terms of the radial distribution function $g(r)$ and of the structure factor $S(k)$. We computed $g(r)$ at a temperature T close to T_M and in the pressure range where reentrant melting occurs. Upon compression, the first peak of $g(r)$ (at $r \simeq \sigma_M$) moves upward while the second and third peaks go down, signalling that more and more particles can overcome the soft-repulsive shoulder (Fig. 3, top panel). This behavior is mirrored in the pressure dependence of $S(k)$ whose main peak first builds up and then goes down (Fig. 3, inset of top panel). This is different from simple fluids, where all $g(r)$ and $S(k)$ peaks get higher as P grows at constant T . We also computed $g(r)$ at a somewhat lower temperature ($T = 10$) and for intermediate pressures. Here, $g(r)$ is highly structured for $r < \sigma$ while it shows an ideal-gas behavior for larger distances (Fig. 3, bottom panel). This suggests that, in the fluid region being considered, particles are grouped in clusters whose linear extent is of the order of σ , with inter-cluster spacing large enough that no significant radial correlations exist between particles in different clusters.

We did not attempt a full analysis of solid polymorphism in the exp-6 system at low temperature, but to a large extent this can be anticipated by the $T = 0$ calculation of the chemical potential (i.e., enthalpy) for a number of relevant crystal structures (see Fig. 4). Optimized structures were computed for the following lattices: FCC, BCC, hexagonal closed packed, simple cubic (SC), simple hexagonal (SH), body-centered tetragonal, plus a few non-Bravais lattices (diamond, BC8, cI16, hR1, and ST12) that occur, either as stable or near-optimal phases, for Li, Na, and Si under high compression^{33,34,35,36}. We found that the sequence of stable phases for increasing pressures is

$$\text{FCC} \xrightarrow{5500} \text{BCC} \xrightarrow{12500} \text{SH} \xrightarrow{19500} \text{BC8} \xrightarrow{31500} \text{SH} \xrightarrow{42500} \text{SC} \xrightarrow{53500} \text{SH} \xrightarrow{72500} \text{FCC}, \quad (2)$$

where the numbers above the arrows indicate the transition pressures (to within a precision of 500). The three separate SH regions correspond to distinct ranges of the ratio c/a between transverse and in-plane lattice parameters, that is 0.69–0.73, 1.33–1.23, and 1, respectively.

In turn, the number of neighbors in close contact with a given particle is 2, 6, and 8. Moreover, at exactly $P = 20000$, the stable BC8 crystal can also be viewed as a cI16 crystal with an internal positional parameter of 0.125. The occurrence of BC8 and cI16 solids (same Pearson symbol³⁷) in light alkali metals has been associated with complex modifications of the electronic density of states^{33,34,38}. Remarkably, our findings show that low-symmetry non-Bravais lattices can be stabilized also for a simple spherically-symmetric classical interaction. The existence of two competing repulsive length scales appears to be an essential ingredient for this surprising result, which discloses the possibility that suitably-tailored colloids (i.e., micrometer-sized particles) may exist as “exotic” solids at standard conditions.

We finally analysed how the phase diagram of the exp-6 model changes with the repulsion steepness by performing calculations for other values of α in the range 10-13. We found that the typical pressure and temperature (\tilde{P}, \tilde{T}) where anomalous features occur do approximately scale as $\epsilon_M(\alpha)/\sigma_M(\alpha)^3$ and $\epsilon_M(\alpha)$, respectively. This amounts to about a tenfold (\tilde{P}) and a fivefold (\tilde{T}) increase per unit α variation. In addition to this major effect, we found that the maximum of $T_m(P)$ becomes more and more pronounced with increasing α .

As illustrated above, the melting behavior of the exp-6 system is related to the gradual switching off, under sufficiently high pressure, of the soft-repulsive length scale in favor of the hard one, which leads to a series of transitions to more and more compact structures. This offers a clue to understand the anomalous melting features of many materials under extreme conditions. As is well known, pressure may trigger a reorganization of the atomic structure, leading to charge transfer to more localized orbitals (see e.g. the 6s-5d transition in Cs⁶). A similar phenomenon is pressure-driven 5p-5d hybridization in Xe³⁹. More often, a pressure-induced symmetry-breaking transition is the large-scale manifestation of a collective response of conduction electrons: upon compression, pseudo-ions will eventually adjust to a new and more compact crystal lattice provided this also ensures an optimum electronic-energy content. Both atomic and structural transitions take place at definite pressures in the solid while in the fluid such changes occur over a broader pressure range. The transition of an element to a more compact solid is usually reflected in a sudden increase of the $T_m(P)$ slope. This is generally preceded by a part of the melting line having negative, vanishing, or very small positive slope. Aside from the specific mechanism at work, such behaviors can be interpreted, in the effective-potential approach, as effects of the weakening of repulsive

forces that is associated with the crossover from a larger to a smaller repulsive length scale. This affects, to a greater or lesser extent, any substance and will induce its structure, at sufficiently high pressure, to settle down on a more compact and stiff arrangement. In some systems, this process may occur repeatedly as pressure increases, which provides a rationale for the behavior hypothesized for K¹⁴ and observed in Sr¹⁰.

The melting behavior that was for long considered as general, i.e., a regularly increasing and concave $T_m(P)$ (typical of e.g. hard-sphere and inverse-power potentials), is actually unrealistic at extreme pressures since it is associated with an essentially rigid-like response to compression. On the contrary, anomalous melting can be expected to be the norm among the elements. However, the pressures and temperatures where structural softening occurs can vary considerably from one substance to the other, as suggested by the sensitive dependence on the repulsion steepness of the location of exp-6 anomalies. In particular, atoms with more electrons should be more susceptible, at least within the same chemical family, to pressure-induced modifications in the condensed phases. This is consistent, for example, with the known properties of alkali metals^{6,7,8,9,11,14} and with the behavior of rare gases, where the flattening observed in the melting line at high pressures is more marked and occurs at a smaller pressure for the heavier gases^{4,39}.

[†] E-mail: malescio@unime.it

[‡] E-mail: saiya@me.cnr.it (corresponding author)

* E-mail: Santi.Prestipino@unime.it

¹ P. F. McMillan, *Nature Materials* **1**, 19 (2002).

² D. A. Young, *Phase diagrams of the elements* (University of California, Berkeley, 1991).

³ S. K. Saxena, G. Shen, and P. Lazor, *Science* **264**, 405 (1994).

⁴ R. Boehler *et al.*, *Phys. Rev. Lett.* **86**, 5731 (2001).

⁵ D. Errandonea *et al.*, *Phys. Rev. B* **63**, 132104 (2001).

⁶ A. Jayaraman, R. C. Newton, and J. M. McDonough, *Phys. Rev.* **159**, 527 (1967).

⁷ F. P. Bundy, *Phys. Rev.* **115**, 274 (1959).

⁸ E. Gregoryanz *et al.*, *Phys. Rev. Lett.* **94**, 185502 (2005).

⁹ J-Y. Raty, E. Schwegler, and S. A. Bonev, *Nature* **449**, 448 (2007).

- ¹⁰ D. Errandonea, R. Boehler, and M. Ross, *Phys. Rev. B* **65**, 012108 (2001).
- ¹¹ E. Rapoport, *J. Chem. Phys.* **48**, 1433 (1968).
- ¹² S. A. Bonev *et al.*, *Nature* **431**, 669 (2004).
- ¹³ G. D. Mukherjee and R. Boehler, *Phys. Rev. Lett.* **99**, 225701 (2007).
- ¹⁴ C.-S. Zha and R. Boehler, *Phys. Rev. B* **31**, 3199 (1985).
- ¹⁵ C. P. Royall *et al.*, *J. Chem. Phys.* **124**, 244706 (2006).
- ¹⁶ F. H. Stillinger, *J. Chem. Phys.* **65**, 3968 (1976).
- ¹⁷ C. N. Likos, *Phys. Rep.* **348**, 267 (2001).
- ¹⁸ S. Prestipino, F. Saija, and P. V. Giaquinta, *Phys. Rev. E* **71**, 050102(R) (2005).
- ¹⁹ G. Malescio, *J. Phys.: Condensed Matter* **19**, 073101 (2007).
- ²⁰ G. Malescio and G. Pellicane, *Nature Materials* **2**, 97 (2003).
- ²¹ P. C. Hemmer and G. Stell, *Phys. Rev. Lett.* **24**, 1284 (1970).
- ²² D. A. Young and B. J. Alder, *Phys. Rev. Lett.* **38**, 1213 (1977).
- ²³ E. A. Jagla, *Phys. Rev. E* **63**, 061501 (2001).
- ²⁴ P. G. Debenedetti, V. S. Raghavan, and S. S. Borick, *J. Phys. Chem.* **95**, 4540 (1991).
- ²⁵ R. A. Buckingham, *Proc. R. Soc. London, Ser. A* **168**, 264 (1938).
- ²⁶ L. E. Fried, W. M. Howard, and P. C. Souers, *Exp-6: a new equation of state library for high pressure thermochemistry*, 12th International Detonation Symposium, August 11-16, 2002 (San Diego, USA).
- ²⁷ M. Ross and A. K. McMahan, *Phys. Rev. B* **21**, 1658 (1980).
- ²⁸ A. B. Belonoshko *et al.*, *J. Chem. Phys.* **117**, 7733 (2002).
- ²⁹ F. Saija and S. Prestipino, *Phys. Rev. B* **72**, 024113 (2005).
- ³⁰ D. Frenkel and B. Smit, *Understanding molecular simulation* (Academic, New York, 2001).
- ³¹ R. Agrawal and D. A. Kofke, *Phys. Rev. Lett.* **74**, 122 (1995).
- ³² P. G. Debenedetti, *Metastable liquids: concepts and principles* (Princeton University Press, Princeton, 1996).
- ³³ J. B. Neaton and N. W. Ashcroft, *Nature* **400**, 117 (1999).
- ³⁴ M. Hanfland *et al.*, *Nature* **408**, 174 (2000).
- ³⁵ M. I. McMahon *et al.*, *Proc. Natl. Acad. Sci. U.S.A.* **104**, 17297 (2007).
- ³⁶ I. Tamblyn, J.-Y. Raty, and S. A. Bonev, *Phys. Rev. Lett.* **101**, 075703 (2008).
- ³⁷ W. B. Pearson, *A Handbook of Lattice Spacings and Structures of Metals and Alloys* (Pergamon,

Oxford, 1967).

³⁸ R. M. Martin, *Nature* **400**, 117 (1999).

³⁹ M. Ross, R. Boehler, and P. Söderlind, *Phys. Rev. Lett.* **95**, 257801 (2005).

FIGURE CAPTIONS

Fig. 1 : The exp-6 potential $u(r)$ for $\alpha = 11$ (solid line, left vertical axis) and the corresponding force $f(r) = -du/dr$ (dashed line, right vertical axis). The force has a maximum strength in the region of the soft-repulsive core. Hence, a new “soft” length scale emerges in the system in addition to the hard-core diameter σ_M . With increasing α , σ_M decreases while ϵ_M gets larger. For instance, when α grows from 11 to 13, σ_M varies from about 0.374σ to 0.245σ whereas ϵ_M varies from about 370ϵ to 7104ϵ .

Fig. 2 : High P -high T phase diagram of the exp-6 model for $\alpha = 11$. Pressure P and temperature T are in units of ϵ/σ^3 and ϵ/k_B , respectively. Coexistence curves are represented as solid lines. Open circles mark coexistence points as estimated through exact free-energy calculations (errors are smaller than the symbols size). The full circle is the outcome of a total-energy calculation. The boundary between the fluid phase and the FCC crystal at extremely high pressures corresponds to the lower stability threshold of the solid. In the intermediate-pressure region (from about 15000 to 70000), additional phases at low temperature are likely present (a BC8 solid, various instances of SH solids, and a SC solid, see text), whose precise boundaries, however, were not computed. The locus of density maxima, $(\partial\rho/\partial T)_P = 0$, in the fluid phase is represented as a dotted line. All lines in the figure are guides to the eye. Inset: reduced number density $\rho\sigma^3$ as a function of temperature for $P = 10000$.

Fig. 3 : Spatial correlations in the exp-6 system for $\alpha = 11$. Top panel: radial distribution function $g(r)$ for $T = 17$; $P = 9000$ (solid line), 12000 (dashed line), 15000 (dotted line), and 18000 (dash-dotted line). Inset: height of the first peak of the structure factor $S(k)$ as a function of pressure at $T = 17$. Bottom panel: $g(r)$ for $T = 10$; $P = 15000$ (dotted line), 20000 (dash-dotted line), 40000 (dashed line), 60000 (solid line).

Fig. 4 : (Color online) $T = 0$ chemical potential μ , plotted as a function of pressure P , for a number of crystal arrangements, choosing the FCC lattice (blue solid line) as a reference (both μ and P are in reduced units; the chemical potentials of structures that are never stable are not shown): BCC (triangles and red solid line), simple cubic (SC, boxes and black solid line), simple hexagonal (SH, dots and light blue solid line),

BC8 (magenta dotted line), and cI16 (green dashed line). The optimized cI16 crystal is actually a BCC crystal up to the pressure where the BC8 solid prevails over BCC. From there onwards, the cI16 line runs over the BC8 line, departing from it only for $P > 20000$.

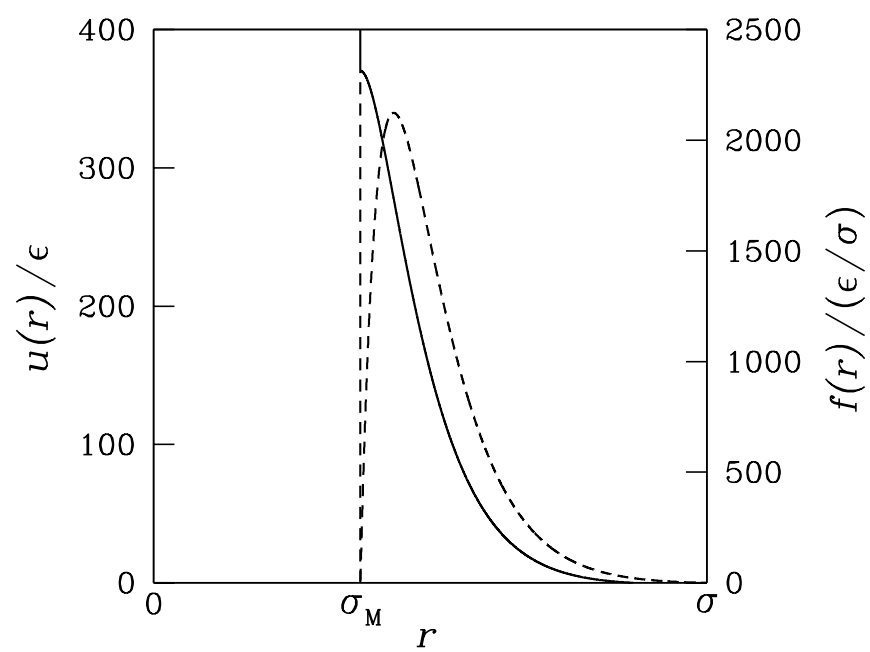


FIG. 1:

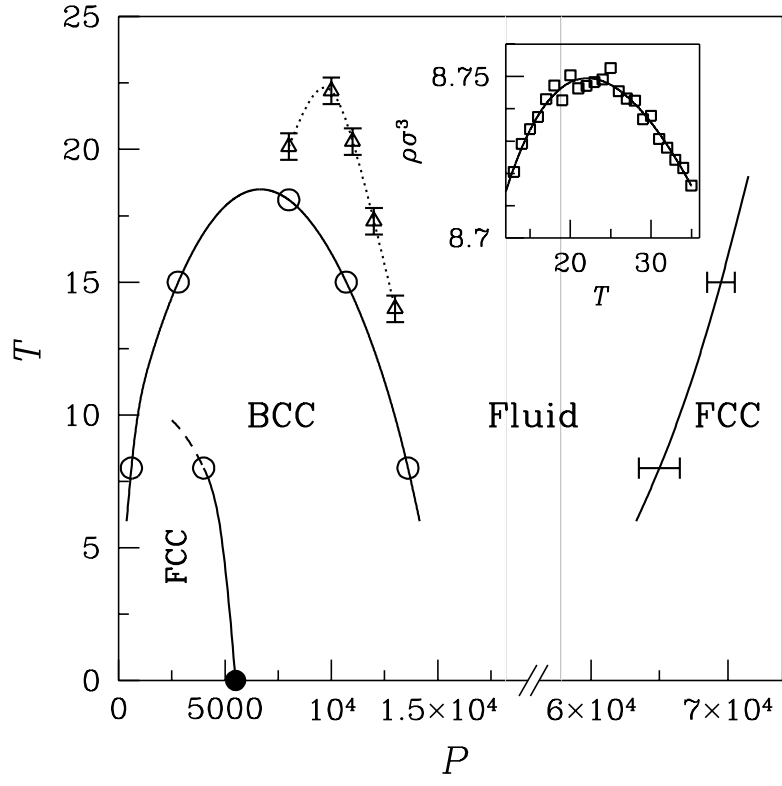


FIG. 2:

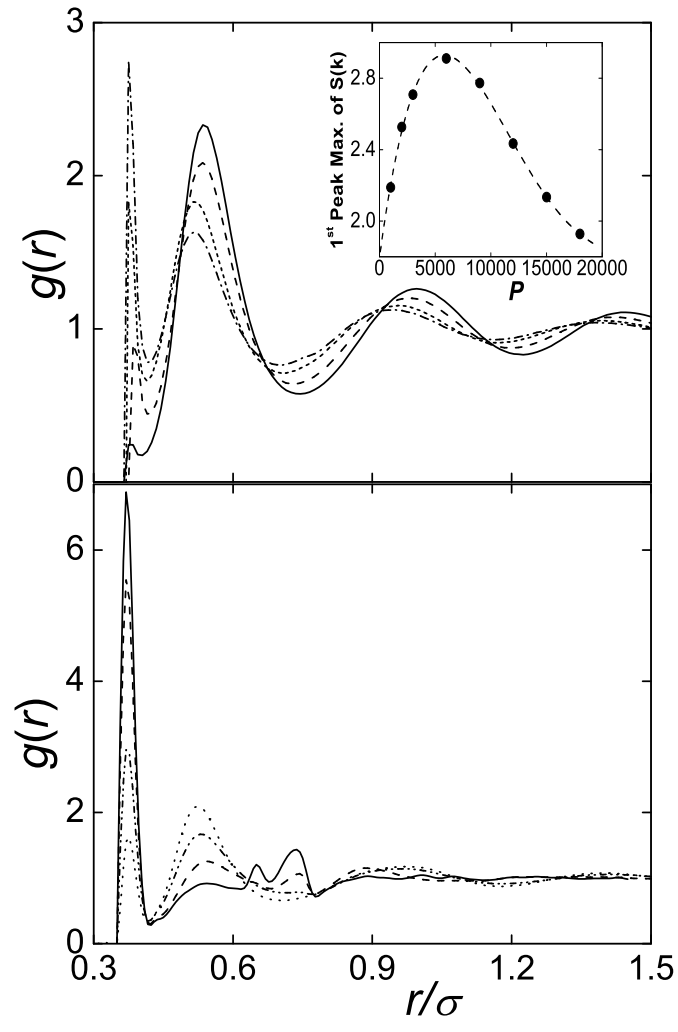


FIG. 3:

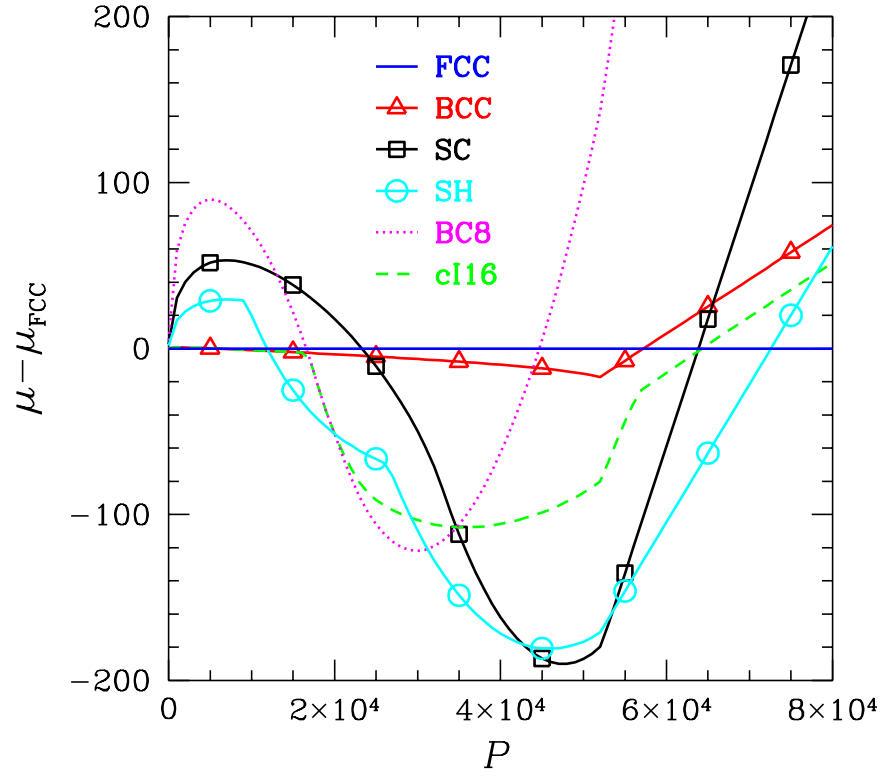


FIG. 4: